



**HAL**  
open science

## Study of the influence of autoclave sterilization on the properties of citrate functionalized iron oxide nanoparticles

Thomas Girardet, Amel Cherraj, Astrid Pinzano, Christel Henrionnet, Franck Cleymand, Solenne Fleutot

► **To cite this version:**

Thomas Girardet, Amel Cherraj, Astrid Pinzano, Christel Henrionnet, Franck Cleymand, et al.. Study of the influence of autoclave sterilization on the properties of citrate functionalized iron oxide nanoparticles. *Pure and Applied Chemistry*, 2021, pp.000010151520210303. 10.1515/pac-2021-0303 . hal-03279293

**HAL Id: hal-03279293**

**<https://hal.science/hal-03279293>**

Submitted on 7 Oct 2021

**HAL** is a multi-disciplinary open access archive for the deposit and dissemination of scientific research documents, whether they are published or not. The documents may come from teaching and research institutions in France or abroad, or from public or private research centers.

L'archive ouverte pluridisciplinaire **HAL**, est destinée au dépôt et à la diffusion de documents scientifiques de niveau recherche, publiés ou non, émanant des établissements d'enseignement et de recherche français ou étrangers, des laboratoires publics ou privés.

# Study of the influence of autoclave sterilization on the properties of citrate functionalized iron oxide nanoparticles.

Thomas Girardet<sup>a</sup>, Amel Cherraj<sup>a</sup>, Astrid Pinzano<sup>b</sup>, Christel Henrionnet<sup>b</sup>, Franck Cleymand<sup>a</sup> and Solenne Fleutot<sup>a\*</sup>

<sup>a</sup> Institut Jean Lamour, Université de Lorraine, CNRS, F-54000 Nancy, France

<sup>b</sup> IMoPA, Université de Lorraine, F-54000 Nancy, France

\* Corresponding author: solenne.fleutot@univ-lorraine.fr

**Abstract:** Superparamagnetic Iron Oxide Nanoparticles (SPIONs) are widely used in various areas of the biomedical field: for diagnosis (Magnetic Resonance Imaging), for therapeutic applications (hyperthermia, nanovectorization). These applications require a good stability in water and no aggregation of SPIONs, with well-controlled physicochemical and magnetic properties. In this work, SPIONs functionalized by citrate ligands are synthesized in a one-step process with the aim of producing stable water-dispersible nanoparticles with a well-crystallized spinel structure. Microwave technology is implemented to achieve this objective given the ease, speed and reproducibility of the method. For their future use in biomedical applications, the sterilization of these SPIONs are essential by an autoclave treatment. The influence of this treatment on the physicochemical and magnetic properties of the SPIONs is determined by a systematic characterization before and after sterilization by Transmission Electronic Microscopy, Dynamic Light Scattering, X-Ray Diffraction, Fourier Transformed Infra-Red, ThermoGravimetric Analysis and magnetic measurements.

**Keywords:** iron oxide nanoparticles, synthesis, functionalization, sterilization, physicochemical properties, magnetic properties

## 1 Introduction

For several decades, nanoparticles (NPs) have been used in different fields: depollution [1], energy storage [2], biomedical applications [3–7]. In this latter field, magnetic NPs at room temperature are often used for diagnosis (contrast agent for MRI) [7], for therapy (hyperthermia) [3] or both [4]. In these cases, magnetic NPs must be biocompatible, stable in aqueous solution and have controlled magnetic properties. To achieve these characteristics, magnetic iron oxide nanoparticles are a good candidate [8,9].

There are several types of magnetic iron oxide NPs including SuperParamagnetic Iron Oxide Nanoparticles (SPIONs) [7,10–12]. For example, with a superparamagnetic state at room temperature, SPIONs are used as a negative contrast agent for MRI for the lymphatic system [10]. SPIONs are conventionally coated with an organic or an inorganic shell to improve their solubility, stability and biocompatibility [13]. Several studies are based on this stability of the iron oxide nanoparticles in aqueous solution using different organic shells: with polymers such as dextran [14], Poly Ethylene Glycol (PEG) [15], Poly Vinyl Pyrrolidone (PVP) [16], chitosan [17] or with small molecules such as citric acid [18], catechol [19].

For biomedical applications, NPs must be sterilized. Two main methods of sterilization exist: terminal sterilization and aseptic processing. The first one is the most used after NPs synthesis [20,21]. There are several methods of terminal sterilization such as sterile filtration [22], UV irradiation [23], chemical sterilization [24], autoclaving [20].

Sterile filtration is used with nanoparticle sizes smaller than the pore size of filter. With the size of the SPIONs in this work, the nanoparticles would be stuck in the filter because this process leads to an agglomeration. With chemical sterilization, organic products like formaldehyde are often used and induce toxicological problems [24]. Finally, autoclaving and UV irradiation are the most widely used sterilization methods because they are easy and quick to use.

In this study, SPIONs covered by an organic citrate shell to stabilize them in aqueous solution are synthesized by a microwave synthesis method. A step of autoclave sterilization is then performed. A study of the evolution of the phys-

icochemical and magnetic properties is carried out before and after treatment to estimate the impacts of these sterilization process.

## 2 Experimental

### 2.1 Materials

Ferrous chloride ( $\text{FeCl}_2 \cdot 4\text{H}_2\text{O}$ ) and ferric chloride ( $\text{FeCl}_3 \cdot 6\text{H}_2\text{O}$ ) were purchased from Alfa Aesar. Citric acid ( $\text{C}_6\text{H}_8\text{O}_7$ ) and ammonium hydroxide solution ( $\text{NH}_4\text{OH}$ ) were purchased from Sigma Aldrich. In all experiment, ultrapure water (resistivity =  $18.2 \text{ M}\Omega \cdot \text{cm}$ ) was used.

### 2.2 Synthesis

A mixture of ferric chloride ( $\text{FeCl}_3 \cdot 6\text{H}_2\text{O}$ ; 3.70 mmol) and ferrous chloride ( $\text{FeCl}_2 \cdot 4\text{H}_2\text{O}$ ; 5.03 mmol) with citric acid ( $\text{C}_6\text{H}_8\text{O}_7$ ; 3.16 mmol) are solubilized in 15 mL of ultra-pure water in a Pyrex reactor for the microwave. This solution is stirred until homogenization. Then, 5 mL of ammonium hydroxide solution is added to the mixture to precipitate the solution. The solution turns black and is stirred again before being placed in the microwave to heat at  $96^\circ\text{C}$  for 40 min. A single-mode microwave (Monowave 400 from Anton Paar) is used. The system operates at a frequency of 2.45 GHz. The maximum power of this microwave is 850 W. The temperature is controlled by an external infrared sensor [25].

After heating, the solution is collected and washed by centrifugation. The solution is centrifuged a first time with ethanol at 10,000 rpm for 5 min and a second time with a mixture of ultrapure water and ethanol at 10,000 rpm for 5 min. The nanoparticles (SPIONs) obtained are then dispersed in ultrapure water. A part is evaporated at  $60^\circ\text{C}$  to obtain powder for X-Ray Diffraction, ThermoGravimetric Analysis and magnetic measurements. The other part is kept in solution for Transmission Electronic Microscopy, Fourier Transformed InfraRed and Dynamic Light Scattering measurements.

### 2.3 Autoclaving

To sterilize SPIONs, an autoclaving treatment is performed at  $120^\circ\text{C}$  during 30 min using an autoclave from Advantage Labo (model AL02-07-100).

### 2.4 Characterization

Different techniques are used for the characterization of nanoparticles.

#### 2.4.1 Transmission Electron Microscopy

Transmission Electron Microscopy (TEM) is used to analyse the shape, size and solvent dispersion of nanoparticles. The TEM is a CM200-FEI operating at 200 kW (point resolution 0.27 nm). The size distribution is calculated using free software ImageJ [26].

### 2.4.2 Dynamic Light Scattering

Dynamic Light Scattering experiments (DLS) were performed by the ZETASIZER Nano ZS device from Malvern Instrumental. The aqueous solution of nanoparticles is diluted one hundred times (final concentration of 0.2 mg/mL) to determine the hydrodynamic size distribution and polydispersity. The isolated or aggregated character of the SPIONs influence the colloidal stability. To evaluate this stability in an aqueous solution, DLS experiments are conducted to determine the average hydrodynamic diameter of the SPIONs in suspension. The DLS measurements are performed three times and the average of these three measurements will be presented in this work.

### 2.4.3 X-Ray diffraction

X-Ray Diffraction (XRD) patterns were recorded in standard conditions with an INEL CPS120 equipped with a monochromatic cobalt radiation ( $\text{Co K}\alpha = 0.17886 \text{ nm}$ ) at grazing angle of incidence simultaneously on  $120^\circ$ . Crystallite size was calculated with the Debye-Scherrer equation from the most intense peak for (311) plane [27].

### 2.4.4 Fourier Transform Infra-Red spectroscopy

Fourier Transform InfraRed analysis (FTIR) were performed with a Nicolet 6700 from Thermo-Fisher between 400 and  $4\,000 \text{ cm}^{-1}$ .

### 2.4.5 Thermogravimetric analysis

ThermoGravimetric Analysis (TGA) were performed on nanoparticle powder to determine the quantity of the organic shell and of the iron oxide core. The device used was a SETSYS EV 1750 TGA microbalance from Setaram. Experiments were conducted in the temperature range of  $20^\circ\text{C}$  to  $600^\circ\text{C}$  under air flow ( $20 \text{ mL/min}$ ) at a heating rate of  $10^\circ\text{C/min}$ .

### 2.4.6 Magnetic measurements

The NPs magnetic properties in powder state were determined by Superconducting Quantum Interference Device (SQUID) with a Vibrating Sample Magnetometer (VSM) Quantum Design head to determine the saturation magnetization ( $M_s$ ) and the blocking temperature ( $T_B$ ). The magnetization was measured by sweeping the magnetic field from  $+5 \text{ T}$  to  $-5 \text{ T}$ , and then from  $-5 \text{ T}$  to  $+5 \text{ T}$ .

Magnetization curves as a function of the temperature were recorded as follows: samples were introduced in the SQUID at room temperature ( $300 \text{ K}$ ) and cooled down to  $5 \text{ K}$  with no applied field after applying a careful degaussing procedure. A magnetic field of  $200 \text{ Oe}$  was then applied, and the magnetization was recorded upon heating from  $5$  to  $300 \text{ K}$  (zero field cooled curves called ZFC curves). The sample was then cooled down to  $5 \text{ K}$  under the same applied field, and the magnetization was recorded upon heating from  $5$  to  $300 \text{ K}$  (field cool curve called FC curves).

## 3 Results and discussion

As the organic citrate layer used in this study is composed exclusively of carbons, oxygen and hydrogen, only the inorganic core is visualized by TEM. The TEM micrographs in Fig. 1 show spherical and isolated SPIONs before (Fig. 1.a) and after (Fig. 1.b) sterilization by autoclaving.

The narrow size distribution histograms are similar before (Fig. 1.c) and after (Fig. 1.d) sterilization. The average particle diameters determined by ImageJ are  $2.10 \pm 1.15$  nm for 2163 counted nanoparticles and  $2.57 \pm 0.99$  nm for 2008 counted nanoparticles respectively before and after sterilization.

TEM analysis of the sterilized or non-sterilized SPIONs show that the sterilization by autoclave doesn't modify the shape, the size and the aggregation state of SPIONs.

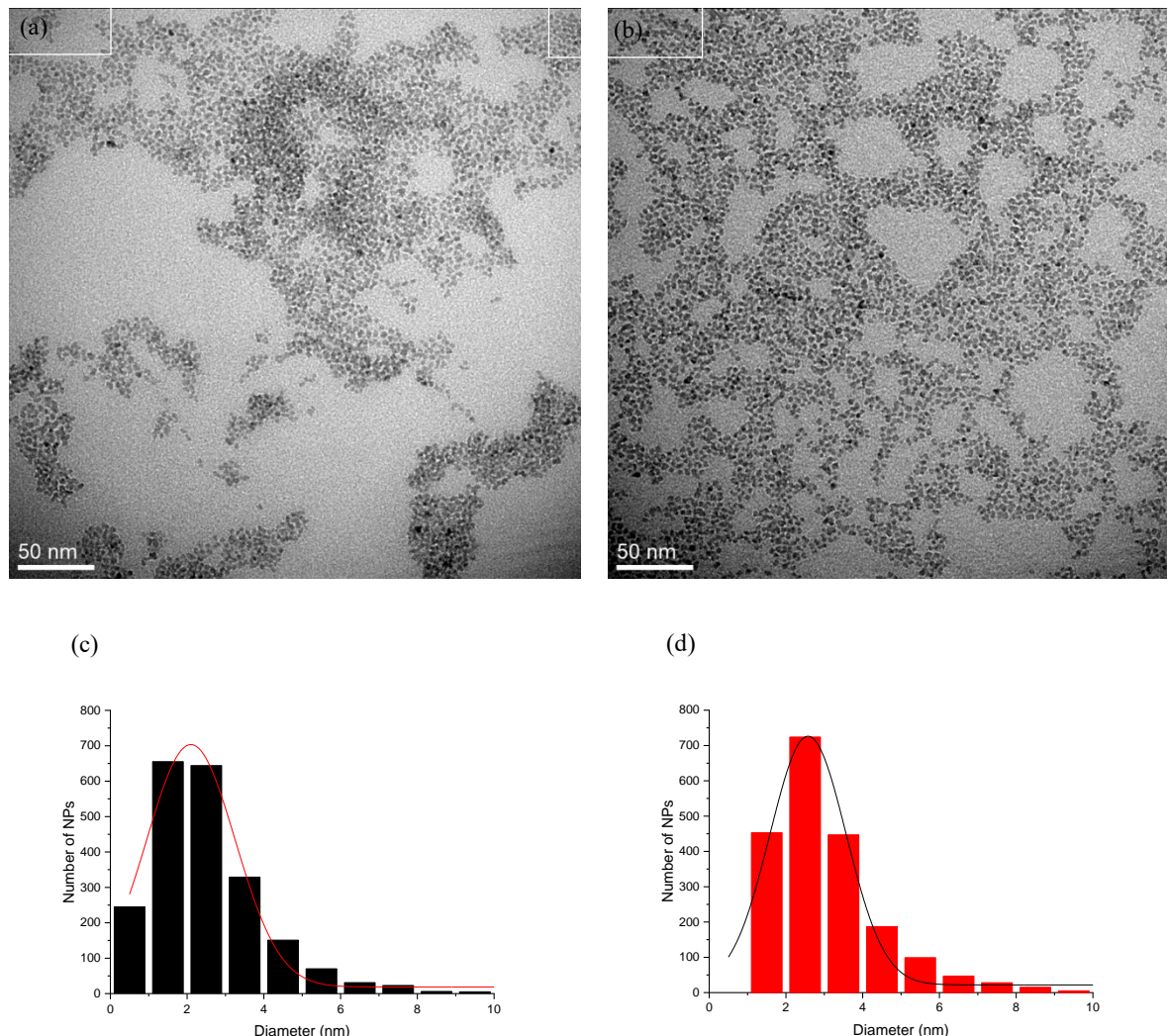


**Fig. 1:** TEM images of SPIONs (a) before and (b) after sterilization by autoclaving with their size distribution histogram respectively in (c) and (d).

Figures 2 present a comparison of size distribution obtained by TEM and DLS. For both, only a population of SPIONs is highlighted. The polydispersity index (PDI) for DLS with small values of 0.29 before treatment and 0.23 after treatment confirms the narrow size distribution obtained by TEM. The mean hydrodynamic diameter corresponds to the maximum of the DLS curve. Figure 2 shows a difference between the diameters determined by TEM on a dry sample and the hydrodynamic diameters measured by DLS in solution. In fact, the hydrodynamic diameter corresponds to the diameter of the mineral shell associated with the thickness of the organic shell and the solvation layer resulting from the interaction between the SPIONs and the aqueous solvent [28]. The hydrodynamic diameter of the SPIONs before (Fig. 2.a) and after (Fig. 2.b) autoclaving is respectively equal to  $8.56 \pm 2.76$  nm and  $8.77 \pm 2.80$  nm. These measurements confirm the conclusions of the TEM analyses. The autoclaving process doesn't modify the nanoparticles size and doesn't induce an aggregation phenomenon.

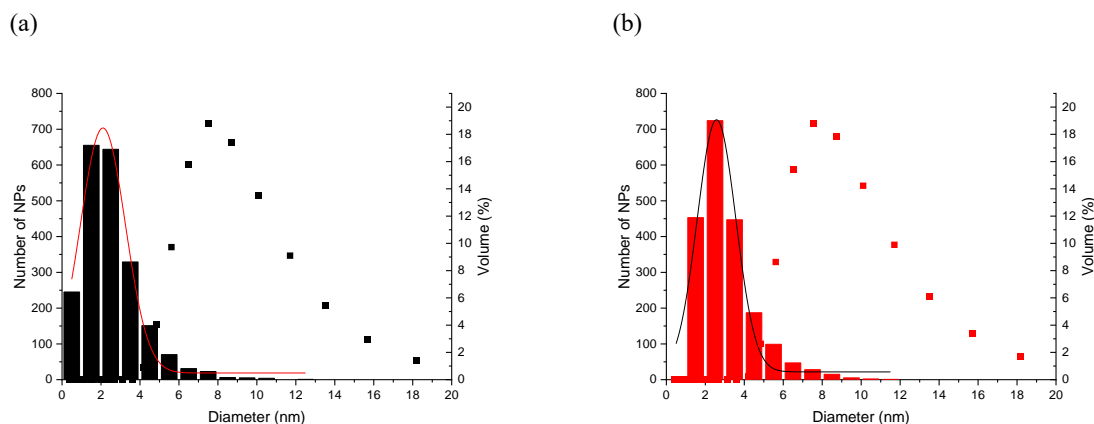


**Fig. 2:** Comparison between average hydrodynamic diameters determined by DLS measurements (point curve) and with size distribution histogram obtained by TEM of SPIONs (a) before and (b) after sterilization.

XRD patterns of SPIONs powder samples show in Fig. 3. Magnetite ( $\text{Fe}_3\text{O}_4$ ) and maghemite ( $\gamma\text{-Fe}_2\text{O}_3$ ) crystallize in a same cubic crystal structure (space group  $F_{d3m}$ ) making it difficult to separate these two structures. Several studies are showed the difference between the XRD pattern of magnetite and of maghemite thanks to the presence of two peaks for the maghemite (corresponding to the appearance of peaks due to vacancies) [6] or thanks to the deconvolution method of some peaks [29].

To determine the influence of sterilization by autoclave on structural properties, the XRD patterns before and after sterilization are compared to a reference of magnetite nanoparticles (JCPDS file: 04-009-2284). The major peaks of the magnetite planes (220), (311), (400), (511) and (440) are present and confirmed the crystallization of the inorganic core. With the Debye Scherrer equation and using the main peak (311), the crystallites size is obtained. The crystallites size is equal to 3.42 nm before sterilization and 3.54 nm after sterilization. The SPIONs sterilization with an autoclave does not influence the crystalline structure.

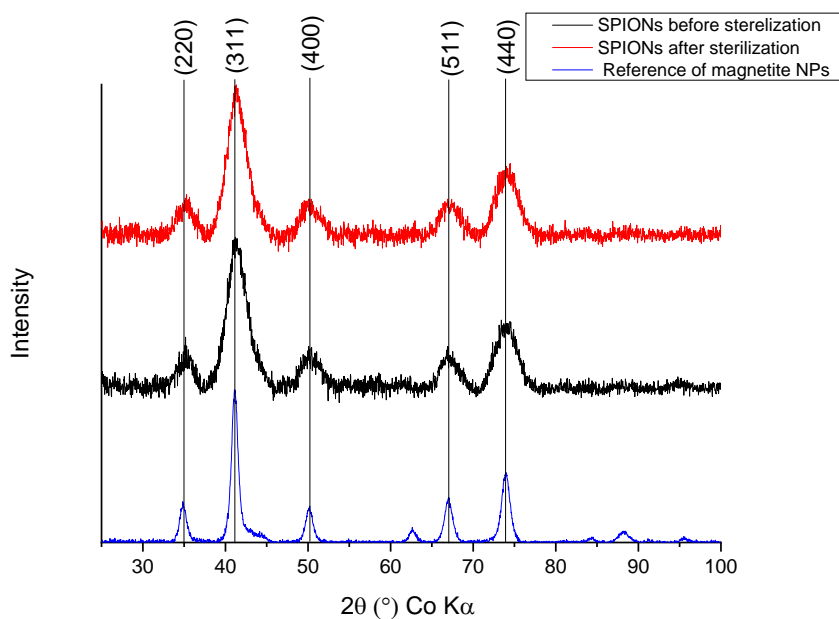


**Fig. 3:** Comparison of XRD patterns of SPIONs before sterilization (black) and after sterilization (red) with XRD pattern of a magnetite NPs reference.

FTIR spectra of SPIONs before and after sterilization, shown in fig 4, can be used to characterize the organic layer and the inorganic core. First, it is important to note that spectra are similar, so the organic layer of SPIONs are not degrade by autoclave sterilization . The large band from  $3500\text{ cm}^{-1}$  to  $2500\text{ cm}^{-1}$  corresponds to the  $\nu(\text{OH})$  of water. The band at  $3200\text{ cm}^{-1}$  is assigned to the  $\nu(\text{NH})$  of free ammonium. The band at  $2800\text{ cm}^{-1}$  corresponds to the  $\nu_s(\text{CH}_2)$ . The bands at  $1610\text{ cm}^{-1}$ ,  $1402\text{ cm}^{-1}$  and  $1064\text{ cm}^{-1}$  are assigned to  $\nu_a(\text{OCO}^-)$ ,  $\delta_s(\text{OCO}^-)$  and  $\nu_s(\text{CO})$  respectively. Finally, the bands at  $632\text{ cm}^{-1}$  and  $580\text{ cm}^{-1}$  corresponds to the elongation of Fe-O bond for maghemite and magnetite respectively [30] .

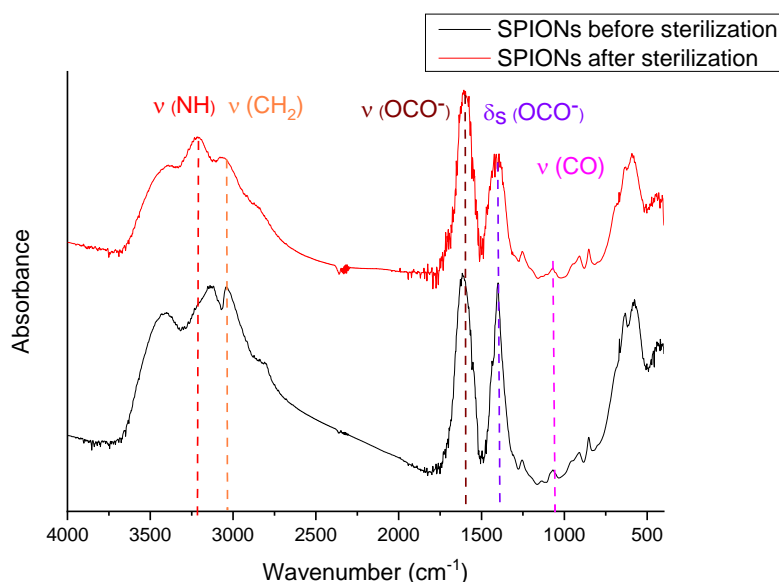


**Fig. 4:** FTIR spectra of SPIONs before (black) and after (red) sterilization between  $4000\text{ cm}^{-1}$  and  $400\text{ cm}^{-1}$ .

To confirm the presence of the organic layer, TGA measurements are realized. The heating curves of SPIONs sample before and after sterilization are shown in Fig. 5. The same behaviour between SPIONs before and after sterilization is observed. In a first time, around  $100^\circ\text{C}$ , a weight loss is present and corresponds to the evaporation of water. Then, a second stage from  $180^\circ\text{C}$  to  $250^\circ\text{C}$  corresponds to the decomposition of citrate. Finally, a last weight loss is produced around  $320^\circ\text{C}$  for the last residues of citrate. The remaining mass corresponds to the mass of iron oxide which was oxidized to hematite ( $\alpha\text{-Fe}_2\text{O}_3$ ). For SPIONs before sterilization, the percentage weight loss is equal to 39% (9% of water and 30% of the organic layer): the remaining mass of the powder is equal to 61% and corresponds to the percentage of iron oxide. For SPIONs after sterilization, the powder contains 62% of iron oxide and 31% of organic layer. Both the TGA and FTIR results confirm the non-degradation of organic layer during the sterilization. Indeed, the autoclave treatment temperature of  $120^\circ\text{C}$  is lower than the decomposition temperature of the citrate observed by thermogravimetric analysis: the autoclave cannot degrade the citrate layer.

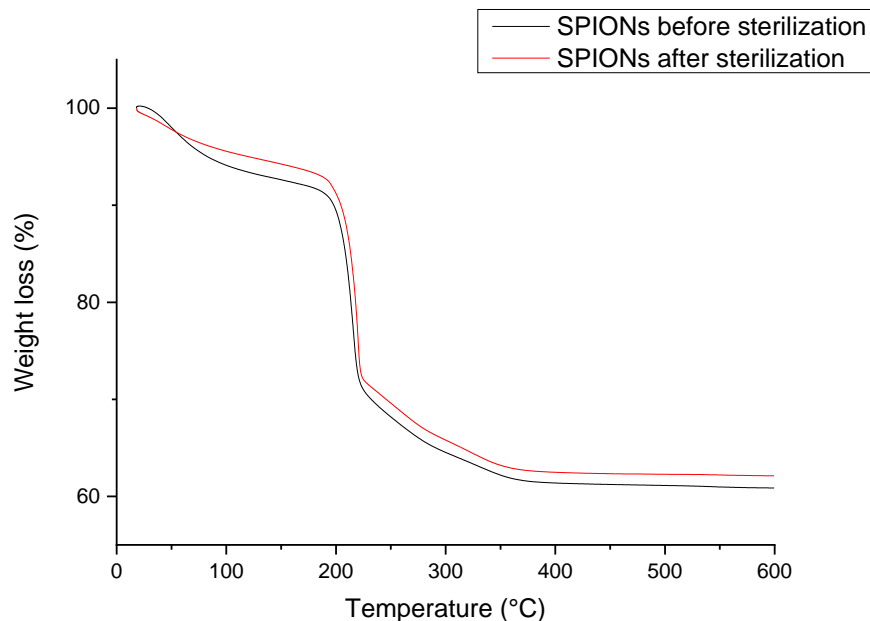


**Fig. 5:** TGA results of SPIONs before sterilization (black) and after sterilization (red) between 20°C and 600 °C.

The magnetization curves  $M(H)$  at 300K and at 5K (with and without a magnetic field during the cooling) are presented in Fig. 6. Without effect of the sterilization, no hysteresis is observed at 300K (Fig. 6.a) which is characteristic of superparamagnetic behaviour. At 300K,  $M_s$  are equal  $54.61 \text{ emu.g}^{-1}$  and  $53.10 \text{ emu.g}^{-1}$  for SPIONs before and after sterilization respectively at 5 T (Fig. 6.a). These values are similar with the  $M_s$  values of SPIONs which are used as a contrast agent in MRI [31–34].

At 5K,  $M_s$  increase and they are equal to  $58 \text{ emu.g}^{-1}$  and  $61 \text{ emu.g}^{-1}$  for SPIONs before and after sterilization respectively at 0.5 T (Fig. 6.b). These values confirm the same size of SPIONs before and after the sterilization treatment.

To evaluate the potential oxidation at the surface of SPIONs, two magnetization curves are realized at 5K: one without magnetic field during the cooling and the second with a magnetic field (4 T) during the cooling.

For SPIONs before and after sterilization (Fig. 6.c and fig 6.d), the left coercive field is similar with or without applied field during the cooling. Sterilization by autoclaving doesn't influence the superparamagnetic properties of iron oxide nanoparticles. If there is an oxidation at the surface, the magnetic state of the surface will be different compared with the magnetic state of the core and nanoparticles will be core-shell structure defined as  $\text{Fe}_3\text{O}_4@\text{Fe}_2\text{O}_3$ . This core-shell structure would be demonstrated by a difference in values between the left coercive field obtained in the 5K cycle without field and with field. No oxidation at the nanoparticle surface is observed after treatment in accordance with the XRD conclusions.

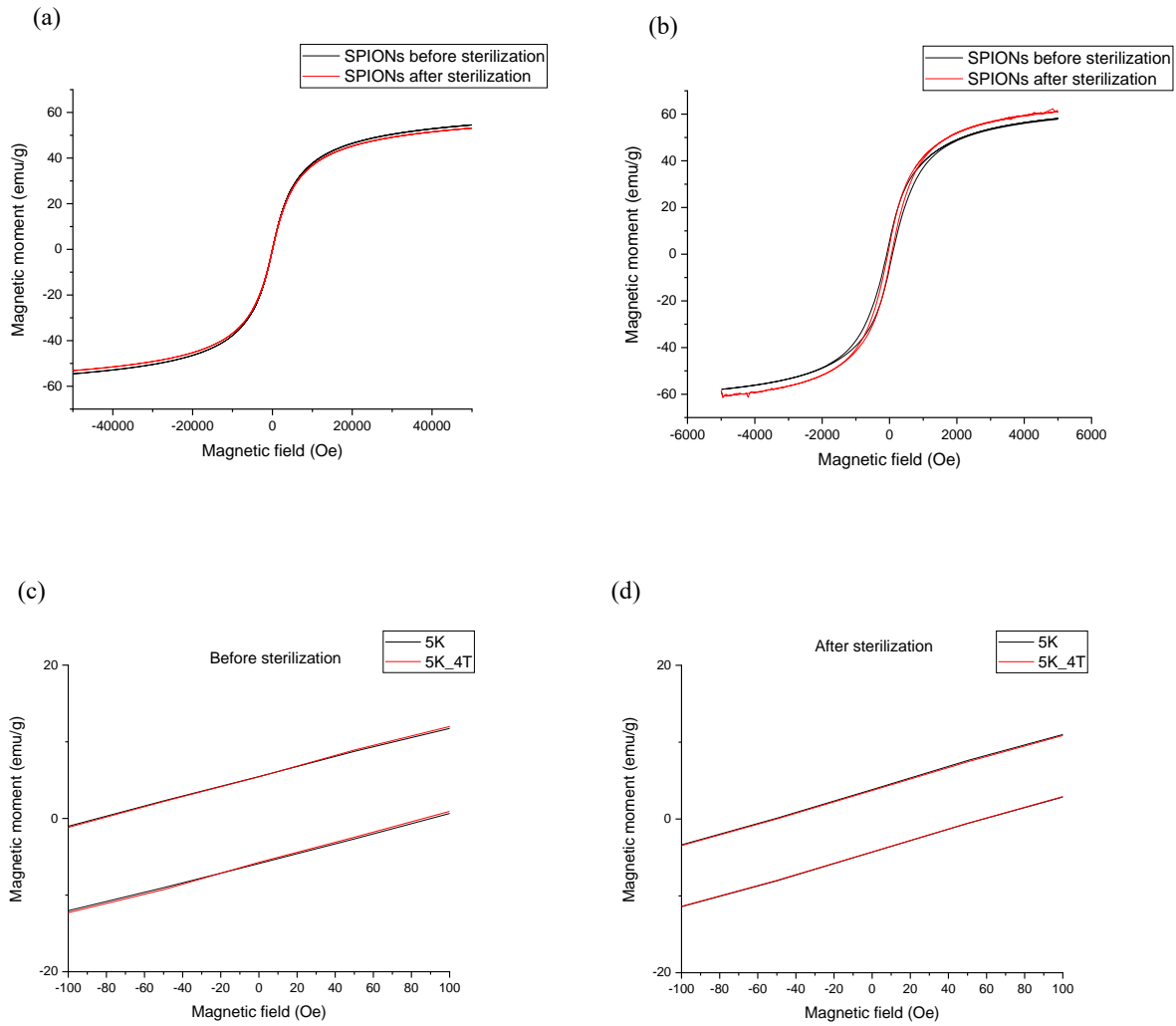


**Fig. 6:** Magnetization curves of SPIONs before (black) and after (red) sterilization as a function of an applied magnetic field at (a) 300K and at (b) 5K. Magnetization curves at 5K without or with applied field during the cooling for SPIONs (c) before sterilization and (d) after sterilization.

To determine the blocking temperature ( $T_B$ ) defined as the temperature transition between the superparamagnetic state and the ferrimagnetic state, ZFC/FC measurements were recorded (Fig. 7).  $T_B$  are assimilated to the maximum of ZFC curves and are equal to 14K and 13K before and after sterilization respectively. These values confirm the superparamagnetic state at 300K and the small sizes of the synthesized SPIONs with a size of nanoparticles proportional to the values of  $T_B$ . In addition, a narrow ZFC curve corresponding to a narrow  $T_B$  distribution confirms a narrow size distribution of the SPIONs. The narrowness of the ZFC curves before and after autoclave process is in agreement with the narrow size distributions obtained in TEM and DLS.

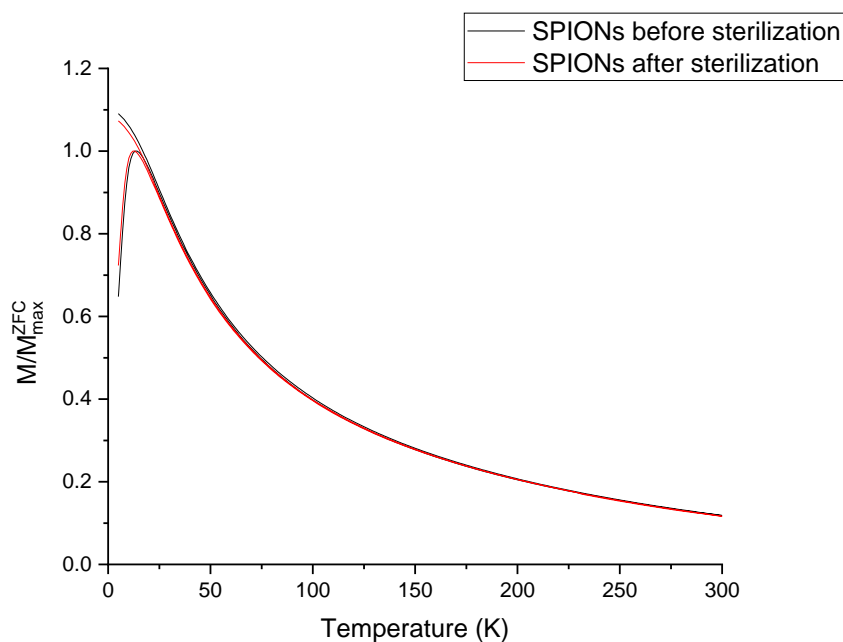


**Fig. 7:** Magnetization as function of the temperature measured under a permanent field of 200 Oe. ZFC-FC curves of SPIONs before (black) and after (red) sterilization.

## 4 Conclusions

SPIONs are synthesized by a one-step microwave method. The nanoparticles obtained by this method present a monodisperse distribution with a narrow size distribution, stable in aqueous solution and exhibit superparamagnetic behaviour, which make them good candidates for biomedical applications. Prior to biomedical applications and *in vitro* contact with cells, an essential step is the sample sterilization. The method used in this study is the autoclave sterilization. A systematic characterization of nanoparticles before and after autoclaving by TEM, DLS, XRD, FTIR, TGA and magnetic measurements has demonstrated that SPIONs keep their physicochemical and magnetic properties after the autoclave treatment. This sterilization treatment doesn't modify the size, morphology or crystal structure of SPIONs. This sterilization does not degrade the organic shell and preserved the surface state of the inorganic core. No additional oxidation is observed. Without aggregation of the nanoparticles after sterilization by this method, the colloidal stability is also preserved. The method of sterilization of SPIONs by autoclave without influence on their physicochemical and magnetic properties is validated before future analysis of cytotoxicity and biocompatibility study.

**Acknowledgments:** We would like to acknowledge the MEM, X-Gamma and Magnetism Competence Centers of Institute Jean Lamour for assistance in TEM, X-ray diffraction and magnetism experiments.

## 5 References

- 1 R. Ortega-Villar, L. Lizárraga-Mendiola, C. Coronel-Olivares, L. D. López-León, C. A. Bigurra-Alzati and G. A. Vázquez-Rodríguez, *J. Environ. Manage.*, **242**, 487–495, 2019.
- 2 J. Peng, W. Zhang, L. Chen, T. Wu, M. Zheng, H. Dong, H. Hu, Y. Xiao, Y. Liu and Y. Liang, *Chem. Eng. J.*, **404**, 126461, 2021.
- 3 S. Laurent, S. Dutz, U. O. Häfeli and M. Mahmoudi, *Adv. Colloid Interface Sci.*, **166**, 8–23, 2011.
- 4 S. Mornet, S. Vasseur, F. Grasset and E. Duguet, *J. Mater. Chem.*, **14**, 2161, 2004.
- 5 A.-H. Lu, E. L. Salabas and F. Schüth, *Angew. Chem. Int. Ed.*, **46**, 1222–1244, 2007.

- 6 W. Wu, Z. Wu, T. Yu, C. Jiang and W.-S. Kim, *Sci. Technol. Adv. Mater.*, **16**, 023501, 2015.
- 7 L. Babes, B. Denizot, G. Tanguy, J. J. Le Jeune and P. Jallet, *J. Colloid Interface Sci.*, **212**, 474–482, 1999.
- 8 C. Corot, P. Robert, J. Idee and M. Port, *Adv. Drug Deliv. Rev.*, **58**, 1471–1504, 2006.
- 9 U. Jeong, X. Teng, Y. Wang, H. Yang and Y. Xia, *Adv. Mater.*, **19**, 33–60, 2007.
- 10 R. Qiao, C. Yang and M. Gao, *J. Mater. Chem.*, **19**, 6274, 2009.
- 11 M. Mahmoudi, S. Sant, B. Wang, S. Laurent and T. Sen, *Adv. Drug Deliv. Rev.*, **63**, 24–46, 2011.
- 12 K. Niemirowicz, KH. Markiewicz, AZ. Wilczewska, H. Car, *Adv Med. Science*, **52**, 196-207, 2012.
- 13 S. Laurent, D. Forge, M. Port, A. Roch, C. Robic, L. Vander Elst and R. N. Muller, *Chem. Rev.*, **108**, 2064–2110, 2008.
- 14 H. D. Do, T. T. H. Le, H. N. Pham and P. T. Ha, *Adv. Nat. Sci. Nanosci. Nanotechnol.*, **10**, 015008, 2019.
- 15 C. Yue-Jian, T. Juan, X. Fei, Z. Jia-Bi, G. Ning, Z. Yi-Hua, D. Ye and G. Liang, *Drug Dev. Ind. Pharm.*, **36**, 1235–1244, 2010.
- 16 O. A. Abu-Noqta, A. A. Aziz and A. I. Usman, *Mater. Today Proc.*, **17**, 1072–1077, 2019.
- 17 J.-B. Qu, H.-H. Shao, G.-L. Jing and F. Huang, *Colloids Surf. B Biointerfaces*, **102**, 37–44, 2013.
- 18 M. E. de Sousa, M. B. Fernández van Raap, P. C. Rivas, P. Mendoza Zélis, P. Girardin, G. A. Pasquevich, J. L. Alessandrini, D. Muraca and F. H. Sánchez, *J. Phys. Chem. C*, **117**, 5436–5445, 2013.
- 19 H. B. Na, G. Palui, J. T. Rosenberg, X. Ji, S. C. Grant and H. Mattoussi, *ACS Nano*, **6**, 389–399, 2012.
- 20 S. Dutz, S. Wojahn, C. Gräfe, A. Weidner and J. Clement, *Nanomaterials*, **7**, 453, 2017.
- 21 L. Li, K. Y. Mak, J. Shi, C. H. Leung, C. M. Wong, C. W. Leung, C. S. K. Mak, K. Y. Chan, N. M. M. Chan, E. X. Wu and P. W. T. Pong, *Microelectron. Eng.*, 310–313, 2013.
- 22 Y. N. Konan, R. Gurny and E. Alléman, *Int. J. Pharm.*, 239–252, 2002.
- 23 Y. Gu, F. Xiao, L. Luo, X. Zhou, X. Zhou, J. Li and Z. Li, *Nanomaterials*, **10**, 18, 2019.
- 24 P. Sommerfeld, U. Schroeder and B. A. Sabel, *Int. J. Pharm.*, **164**, 113–118, 1998.
- 25 P. Venturini, S. Fleutot, F. Cleymand, T. Hauet, J. Dupin, J. Ghanbaja, H. Martinez, J. Robin and V. Lapinte, *ChemistrySelect*, **3**, 11898–11901, 2018.
- 26 M.D. Abràmoff, P.J. Magalhães, S.J. Ram, *Biophotonics International*, 36-32, 2004.
- 27 P. Graveriau, Introduction à la pratique de la diffraction des rayons X par les poudres., 3rd edn., 2011.
- 28 J. Lim, S. P. Yeap, H. X. Che and S. C. Low, *Nanoscale Res. Lett.*, **8**, 381, 2013.
- 29 W. Kim, C.-Y. Suh, S.-W. Cho, K.-M. Roh, H. Kwon, K. Song and I.-J. Shon, *Talanta*, 348–352, 2012.
- 30 S. Nigam, K. C. Barick and D. Bahadur, *J. Magn. Magn. Mater.*, 237–243, 2011.
- 31 A. M. Predescu, E. Matei, A. C. Berbecaru, C. Pantilimon, C. Drăgan, R. Vidu, C. Predescu and V. Kuncser, *R. Soc. Open Sci.*, **5**, 171525, 2018.
- 32 N. Ohannesian, C. T. De Leo and K. S. Martirosyan, *Mater. Today Proc.*, **13**, 397–403, 2019.
- 33 G. Kandasamy and D. Maity, *Int. J. Pharm.*, **496**, 191–218, 2015.
- 34 Y. Wu, Z. Lu, Y. Li, J. Yang and X. Zhang, *Nanomaterials*, **10**, 1441, 2020.